Nat Cell Biol. Author manuscript; available in PMC 2011 November 01.

Published in final edited form as:
Nat Cell Biol. 2011 May ; 13(5): 589–598. doi:10.1038/ncb2220.

During autophagy mitochondria elongate, are spared from degradation and sustain cell viability

Ligia C. Gomes[1,2,3], **Giulietta Di Benedetto**[2,4], and **Luca Scorrano**[1,2,5]

[1]Dulbecco-Telethon Institute [2]Venetian Institute of Molecular Medicine, Via Orus 2, 35129 Padova, Italy [3]PhD Programme in Experimental Biology and Biomedicine, Center for Neuroscience and Cell Biology, University of Coimbra, 3004-517 Coimbra, Portugal [4]CNR Institute for Neurosciences, Section of Padova, Via G. Colombo 3, 35129 Padova, Italy [5]Department of Cell Physiology and Medicine, University of Geneva, 1 Rue M. Servet, 1211 Geneve, Switzerland

Summary

A plethora of cellular processes, including apoptosis, depend on regulated changes in mitochondrial shape and ultrastructure. Scarce is our understanding of the role of mitochondria and of their morphology during autophagy, a bulk degradation and recycling process of eukaryotic cells' constituents. Here we show that mitochondrial morphology determines the cellular response to macroautophagy. When autophagy is triggered, mitochondria elongate in vitro and in vivo. Upon starvation cellular cAMP levels increase and protein kinase A (PKA) becomes activated. PKA in turn phosphorylates the pro-fission dynamin related protein 1 (DRP1) that is therefore retained in the cytoplasm, leading to unopposed mitochondrial fusion. Elongated mitochondria are spared from autophagic degradation, possess more cristae, increase dimerization and activity of ATP synthase, and maintain ATP production. When elongation is genetically or pharmacologically blocked, mitochondria conversely consume ATP, precipitating starvation-induced death. Thus, regulated changes in mitochondrial morphology determine the fate of the cell during autophagy.

Introduction

Mitochondria are crucial organelles for energy production, regulation of cell signaling and amplification of apoptosis. This functional versatility is matched by their morphological and structural variety. During cell life, the mitochondrial network is continuously shaped by fission and fusion events[1]. The dynamin-related GTPases optic atrophy 1 (OPA1) of the inner mitochondrial membrane[2], and mitofusins (MFN) 1 and 2 of the outer membrane[3], regulate mitochondrial fusion in mammalian cells. Mitochondrial fission is controlled by the cytosolic dynamin related protein DRP1[4]. Translocation of DRP1 to mitochondria is an essential step in the fragmentation of the organelle and depends on dephosphorylation of the Ser637 residue, by calcineurin[5]. Conversely, phosphorylation of Ser637 by PKA promotes mitochondrial elongation[6],[7]. Once on mitochondria, DRP1 can be stabilized by SUMOylation[8] mediated by resident SUMO ligases such as MAPL[9], elucidating how dynamic regulation of fission adapts mitochondrial morphology to the changing cellular needs.

Address correspondence to: Luca Scorrano. luca.scorrano@unige.ch.

Authors' contributions

LCG and LS conceived research, analyzed data and wrote the manuscript. LCG, GDB, LS performed experiments and analyzed data.

Europe PMC Funders Author Manuscripts

The availability of genetic tools allowed to explore the role of mitochondrial morphology in complex cellular processes. For example, remodelling of mitochondrial cristae[10] and fragmentation of the organellar network[11],[12] participate in the progression of apoptosis. More recently, Ca^{2+} signalling[13], formation of dendritic spines[14], migration of lymphocytes[15], cell cycle[16], and even lifespan in lower eukaryotes[17] have been found to depend on regulated changes in mitochondrial morphology. Finally, mitophagy, a particular form of selective autophagy of mitochondria, requires fragmentation of the mitochondrial network to segregate the dysfunctional units to be removed[18],[19].

Autophagy is a self-degradation process induced for example when nutrients are limited[20]. During autophagy, pre-autophagosomal structures engulf components of the cytosol, including entire organelles, giving rise to autophagosomes that ultimately fuse with lysosomes, where breakdown of cellular components takes place[21]. For many years, autophagy has been regarded as an unselective process, but it is now clear that under certain conditions specific cargoes are selectively targeted to autophagy, including aggregated proteins[22], invading bacteria[23], as well as superfluous or damaged organelles like peroxisomes[24], endoplasmic reticulum[25] and mitochondria[26]. Not only organelles can be selectively eliminated by autophagy, but they also participate in the different steps of macroautophagy, ranging from the formation of the autophagosomal membrane[27], to the amplification of the process, in which mitochondria-derived reactive oxygen species seem to play a role[28]. Mitochondria might also serve as docking sites for the formation of the autophagosomes[29] in a process that depends on the tethering to the endoplasmic reticulum[30]. However, many questions on the morphology as well as on the functional role of mitochondria during autophagy remain open. Do they fragment? Are they randomly targeted to autophagosomes? Is the progression or the final outcome of autophagy influenced by changes in their morphology? Here we show that mitochondria unexpectedly elongate during macroautophagy. Mitochondrial elongation is triggered by the PKA-mediated inhibition of the pro-fission protein DRP1 and is required to sustain cellular ATP levels and viability. Our results indicate that mitochondrial shape determines the cellular fate during macroautophagy.

Results

Mitochondria elongate upon induction of autophagy

We assessed whether mitochondrial morphology is modified during autophagy. Confocal microscopy of wild type (wt) mouse embryonic fibroblasts (MEFs) expressing a mitochondrially targeted yellow fluorescent protein (mtYFP) showed that induction of autophagy by starvation led to an early elongation of mitochondria resulting in a network of highly interconnected organelles (Fig. 1a,b). Elongation was observed as soon as 1 hr after nutrient deprivation, was maintained for up to 48 hrs (not shown) and occurred in all the cell lines tested (mouse C2C12 myoblasts, human HeLa epithelial and HepG2 hepatocarcinoma cells) as well as in primary mouse hepatocytes (Fig. S1a). Inactivation of the mTOR metabolic sensor is another classical stimulus of autophagy. Efficient short RNA interference mediated knock down of mTOR also triggered mitochondrial elongation (Fig. 1c,d). The dilution rate of a mitochondrially targeted photoactivable green fluorescent protein (mt-PAGFP) is proportional to productive fusion events[31]. Dilution rate increased upon starvation in wt as well as *Mfn2*$^{-/-}$ cells (Fig. 1e-g and Movie 1). Accordingly, induction of autophagy led to mitochondrial elongation in *Mfn2*$^{-/-}$, but not in *Opa1*$^{-/-}$[32] and *Mfn1*$^{-/-}$*Mfn2*$^{-/-}$ (*DMF*$^{-/-}$)[33] MEFs, which lack the core components of the mitochondrial fusion machinery; and mitochondria remained elongated in *Drp1*$^{-/-}$ cells where fission is genetically impaired[34] (Fig.1a,b). BAX and BAK have been described to be necessary for fusion of mitochondria[18] and in their absence autophagy is enhanced as a default death mechanism[19]. In response to starvation, the *Bax*$^{-/-}$*Bak*$^{-/-}$ punctiform mitochondria also

elongated (Fig. S1c,d), indicating that BAX and BAK are not essential for elongation during induction of autophagy. In all the MEFs tested, autophagic flux measured in the presence of bafilomycin A1 was comparable, as judged by processing of LC3-I to LC3-II and by degradation of p62 (Fig. S2). In addition, mitochondrial elongation during starvation was still observed when proximal autophagic signalling was blocked by wortmannin (Fig. S3) and in cells lacking the key component of the autophagic machinery ATG5 (not shown). When autophagy was induced *in vivo* by fasting mice for 12 hrs, electron microscopy (EM) of muscle and liver revealed similar changes in mitochondrial morphology. Longitudinal sections of *tibialis anterior* from fasted mice showed that intermyofibrillar mitochondria were retrieved as one elongated organelle, no longer surrounded by glycogen granules; also in liver, perinuclear mitochondria were clearly elongated in fasted mice (Fig. 1h). In sum, mitochondrial elongation requires the core mitochondrial fusion machinery and is not dependent on autophagosome formation, which is conversely independent from mitochondrial elongation.

Mitochondrial elongation during autophagy depends on DRP1 phosphorylation by PKA

Mitochondrial hyperfusion can be triggered by a panoply of stress stimuli and depends on changes in OPA1 forms[20]. In response to starvation, however, levels of total as well as of individual forms of OPA1 were stable, like those of MFN1, MFN2, and FIS1. The total amount of the fission protein DRP1 was slightly increased (Fig. 2a-d), but less DRP1 was associated with mitochondria in the course of starvation (Fig. 1e). This result suggests that during starvation mitochondrial fusion is left unopposed. The PKA/calcineurin couple regulates phosphorylation of the Ser637 residue of DRP1, its translocation to mitochondria and therefore the intensity of mitochondrial fission[5]. Notably, in the course of starvation phosphorylation of Ser637 of DRP1 was increased (Fig. 2f,g). Similarly, silencing of mTOR or its pharmacologic inhibition resulted in increased Ser637 phosphorylation (Fig. 2h,i). This phosphorylation could result from PKA activation or calcineurin inhibition: we therefore examined levels of the proximal PKA activator cAMP in response to starvation using a genetically encoded EPAC-based FRET probe for cAMP. Real time imaging reported a robust increase in cAMP levels in MEFs when switched from a nutrient-rich to the “starvation” medium (Fig. 3a,b). This increase resulted in the downstream activation of PKA, as measured by the phosphorylation of the PKA targets CREB and ATF1, sensitive to H89, a pharmacological inhibitor of PKA (Fig. 3c). Activation of PKA was detected in all the other cell lines (mouse C2C12, human HeLa and HepG2), where starvation induced mitochondrial elongation (Fig. S1b). PKA activation was comparable in cells where mitochondria did (wt and $Mfn2^{-/-}$) and did not ($Opa1^{-/-}$ and $DMF^{-/-}$) elongate in response to starvation (Fig. 3c), indicating that activation does not depend on the mitochondrial morphology. The PKA inhibitor H89 blocked mitochondrial elongation during starvation (Fig. 3d,e), suggesting that PKA activation is conversely an essential step for mitochondrial elongation. Consistently, an increase in cAMP levels obtained pharmacologically led to mitochondrial elongation (Fig. S4). To test if the activation of PKA impinged on Drp1, we turned to a genetic approach. In MEFs expressing a Drp1-YFP chimera mutated in the PKA phosphorylation site ($DRP1^{S637A}$-YFP)[5], mitochondria were unable to elongate during starvation, and inhibition of PKA had no effect on morphology (Fig. 3f,g). Finally, we reconstituted $Drp1^{-/-}$ MEFs with levels of DRP1-YFP or $DRP1^{S637A}$-YFP comparable to those of endogenous DRP1. In the reconstituted cells mitochondria reverted to short rods and starvation could induce H89-sensitive elongation only when MEFs were complemented with Drp1-YFP but not with $DRP1^{S637A}$-YFP (Fig. 3h,i). Thus, during starvation the activation of PKA impinges on DRP1 to trigger mitochondrial elongation.

Elongated mitochondria are spared from autophagic degradation and maintain ATP levels during starvation

Fragmentation of dysfunctional mitochondria precedes mitophagy, suggesting a role for mitochondrial elongation during autophagy in maintenance of the mitochondrial mass. Following starvation, mitochondrial proteins (cyclophilin D, MnSOD and a subunit of complex II) were lost more rapidly in *Opa1*$^{-/-}$ (Fig. 4a) and *DMF*$^{-/-}$ (Fig. 4b) cells that did not elongate mitochondria, while were retained in *Drp1*$^{-/-}$ cells (Fig. 4c,d). These quantitative immunoblotting data were confirmed by a confocal analysis of colocalization[30] of mitochondria with YFP-LC3 labelled autophagosomes (Fig. S5). No differences were observed in the rate of degradation of proteins from other sub-cellular compartments (the peroxisomal marker PMP70 and the cytosolic protein actin). Furthermore, wortmannin that blocks autophagosome formation prevented mitochondrial elimination, supporting that mitochondria were degraded by autophagy (Fig. 4e). Increased degradation could be supported by dysfunction of *Opa1*$^{-/-}$ mitochondria during starvation. While during starvation the accumulation of the potentiometric fluorescent dye tetramethyl rhodamine methylester resulted higher in *Opa1*$^{-/-}$ cells (Fig. S6a), an assay for latent mitochondrial dysfunction revealed that mitochondria of starved *Opa1*$^{-/-}$ MEFs maintain their membrane potential by using the reversal of the ATPase[21] (Fig. 5a,b). Accordingly, total cellular ATP levels decreased in *Opa1*$^{-/-}$ and *DMF*$^{-/-}$ cells during starvation (Fig. 5c). Reduced mitochondrial ATP production contributed to these decreased total cellular ATP levels, while wild-type organelles where elongation occurs were able to sustain ATP output, as indicated by monitoring of mitochondrial ATP levels in situ using a genetically encoded luciferase probe targeted to the matrix of the organelle[35] (Fig. 5d). The free energy of the electrochemical potential is used by the mitochondrial ATPase to synthesize ATP[36]. Although isolated ATPase is fully active as a monomer, the enzyme is ubiquitously found in more efficient dimeric and oligomeric forms[37]. Blue-native gel electrophoresis performed on whole cells allowed to inspect the ATP synthase organization and activity during starvation without isolating mitochondria (and therefore disrupting their morphology). The total levels of ATP synthase increased upon starvation as indicated by specific immunoblotting (Fig. S6b). In wt but not *Opa1*$^{-/-}$ or *DMF*$^{-/-}$ MEFs the ratio between the dimeric and the monomeric form of the ATPase was higher already in non starved cells and increased during starvation, as judged by a specific in gel activity assay for ATPase activity (Fig. 6). Dimerization of ATPase correlates with formation of cristae[37],[38]. However, the reverse can also be true, that increased cristae surface favors oligomerization of the ATPase. Electron microscopy and morphometric analysis showed that the number of cristae per unit of mitochondrial surface increased during starvation in wt and *Mfn2*$^{-/-}$ mitochondria that elongate, while it remained stable in *Opa1*$^{-/-}$ and *DMF*$^{-/-}$ mitochondria that do not (Fig. 7a-c). Thus, during starvation mitochondrial elongation correlates with increased cristae surface, oligomerization of the ATPase and maintenance of mitochondrial ATP production.

Mitochondrial elongation protects cells from death during starvation

What is the role of starvation-induced elongation in the cellular response to nutrient depletion? *Opa1*$^{-/-}$ and *DMF*$^{-/-}$ as well as cells where PKA was inhibited (Fig. 5e-g) died more rapidly, whereas *Drp1*$^{-/-}$ MEFs were less susceptible to starvation (Fig. 5h). The increased death by starvation of cells treated with H89 was phenocopied in *Drp1*$^{-/-}$ MEFs complemented with the mutant of Drp1 in the PKA site (Fig. 5i). Knock down of *OPA1* in HeLa cells also accelerated starvation-induced cell death (Fig. S7a,b). Death of *Opa1*$^{-/-}$ and *DMF*$^{-/-}$ MEFs was prevented by the ATPase inhibitor oligomycin (Fig. 5j,k), in accordance with the fact that mitochondria unable to elongate during starvation maintain their membrane potential by hydrolyzing and consuming cellular ATP (Fig. 5b,c). In conclusion, mitochondria unable to elongate during nutrient deprivation consume cellular ATP, leading to cell death.

Discussion

We have demonstrated that during starvation mitochondria elongate and that this is a critical component of the cellular response to autophagy. In starving cells, a rapid increase in cAMP levels activates PKA that in turn phosphorylates the pro-fission molecule Drp1, keeping it in the cytosol and allowing unopposed mitochondrial fusion. Elongated mitochondria are protected from autophagic elimination, display denser cristae where ATPase can oligomerize to maintain ATP production and to allow survival of starving cells. On the contrary, if elongation is blocked mitochondria become dysfunctional and "cannibalize" cytoplasmic ATP to maintain their membrane potential, precipitating cell death (see model in Fig. 8).

Macroautophagy triggered by nutrient deprivation degrades different constituents of the cell to allow their recycling. If mitochondria were also to be targeted to the autophagosome, their fragmentation should precede engulfment, as it occurs during selective mitochondrial autophagy[18]. However, in response to stimuli that induce macroautophagy, mitochondria elongate as a consequence of Drp1 phosphorylation at Ser637 by PKA, triggered by an increase in cAMP levels. Interestingly, glucagon, the prototypical inducer of autophagy in liver, induces cAMP elevation in hepatocytes[39]. Here we extend the importance of cAMP in autophagy by starvation in tissues other than liver. In yeast activation of PKA is important in pseudohyphal differentiation triggered by nitrogen starvation[40] Conversely, constitutive activation of PKA inhibits autophagosome formation[41],[42] suggesting that the PKA loop elucidated here might be specific for higher eukaryotes. Along this line, the yeast orthologue of DRP1 lacks a conserved PKA phosphorylation site, suggesting that the metabolic response of yeast mitochondria during autophagy is differentially regulated. Elongation and phosphorylation of DRP1 occurs also in response to inactivation of the metabolic sensor mTOR, suggesting an interplay with PKA that is supported in different paradigms in mammals[43] and in yeast[44]. Several mechanisms are responsible for the changes in mitochondrial shape triggered by external and internal cues: for example, in cells exposed to several stresses, a change in the relative levels of the forms of the pro-fusion OPA1 support mitochondrial elongation[45], while during apoptosis mitochondrial fragmentation is supported by the concerted action of inhibition of mitochondrial fusion[46], by the stimulation of DRP1 translocation to mitochondria[47], where it is stabilized by a Bax, Bak dependent process of SUMOylation[48]. Conversely, during starvation the forms of OPA1 remain stable, but mitochondrial levels of DRP1 are reduced. Multiple biochemical and genetic evidence support that the reduced levels are a consequence of its phosphorylation by activated PKA. Alternatively, another interesting possibility could be that during macroautophagy mitochondrial DRP1 is not stabilized by SUMOylation, being then ubiquitinated by resident mitochondrial ubiquitin ligases[49],[50], and degraded in a proteasome-dependent fashion. Along this line, upon induction of mitophagy the ubiquitin ligase Parkin degrades components of the mitochondrial fusion machinery[51],[52] and targets dysfunctional organelles to the autophagosome[53]. However, starvation induced mitochondrial elongation occurs also in HeLa cells where Parkin is not expressed[53], further substantiating the key role of the cAMP-PKA-DRP1 loop in autophagy. Opposed to the "active" adaptation of mitochondrial morphology to the cellular cues described here, lies the pathological DRP1-mediated fragmentation by sustained activation of calcineurin like that observed in Huntington's disease which results in increased susceptibility to apoptotic insults[54]. These two extremes elucidate how mitochondrial morphology is extremely sensitive to, and plastically modulated by cellular inputs.

Why do mitochondria elongate during induction of autophagy? Elongated mitochondria are spared from autophagy, implying that the "targets" for degradation during macroautophagy might not be random. The limitation could be simply sterical –i.e. the elongated

mitochondria can not fit into the autophagosome. Alternatively, longer mitochondria might lack the signal that addresses them to the autophagosome. In this respect, it is interesting to note that shorter mitochondria are not only less efficient in ATP production, but they also bear a latent dysfunction that could trigger the relocalization of Parkin on their surface[53]. Teleologically speaking, one could wonder why macroautophagy spares mitochondria. During nutrient restriction, cells try to maximize efficiency of energy conversion, a task perfectly performed by mitochondria[55] and that requires mitochondrial elongation, as we showed here. Elongated mitochondria display higher levels of dimers of the ATPase, associated with increased efficiency in ATP production[37]. Morphologically, this is mirrored by an increase in the number of cristae, the privileged compartments for ATP synthesis[37], per mitochondrial surface. While OPA1 and cristae organization are directly linked[56],[57], it is less clear why *DMF*$^{-/-}$ MEFs are unable to respond to starvation with an increase in cristae biogenesis. However, OPA1 forms are altered in *DMF*$^{-/-}$ MEFs and knock down of DRP1 similarly alters processing of OPA1[58]. Thus, it appears that processing of OPA1 (and hence biogenesis of the cristae) are exquisitely sensitive to changes in the fusion-fission equilibrium, ultimately impacting on the ability of the mitochondria to metabolically respond to the environment. In addition, mitochondria could be essential to provide membranes for the formation of the autophagosome[29] and they should therefore be excluded from immediate degradation, in order to ensure the progression of the autophagic process.

During starvation, mitochondria unable to elongate are latently dysfunctional and they consume cytosolic ATP to sustain their membrane potential. The ensuing bioenergetic crisis due to ATP consumption causes starvation-induced cell death in *Opa1*$^{-/-}$ and *DMF*$^{-/-}$ MEFs. As expected, during starvation autophagy is essential to provide nutrients and its blockage accelerates death[59], irrespective of whether mitochondrial elongation occurs or not. Whether the protective role of autophagy is a general feature of all forms of cell death remains a matter of intense debate. Our data conversely indicate that changes in mitochondrial morphology and function are an essential subroutine of the autophagic program: if a stereotypical response of the cell (mitochondrial elongation and activation) to limited nutrient supply is abolished, the ensuing mitochondrial dysfunction can lead to cell death. The unexpected role of mitochondrial elongation during starvation exemplifies a further cellular response regulated by these organelles.

Supplementary Material

Refer to Web version on PubMed Central for supplementary material.

Acknowledgments

L.C.G. is the recipient of a “Bolsa de Doutoramento” of the “Fundação para a Ciência e Tecnologia”, Portugal. L.S. is a Senior Telethon Scientist of the Dulbecco-Telethon Institute. This research was supported by Telethon Italy S02016, AIRC Italy, Swiss National Foundation SNF 31-118171. We thank D.Chan, K. Mihara, C. Blackstone, N. Mizushima for reagents; T. Pozzan for helpful discussion on mt-luciferase calibration.

Appendix

Methods

Molecular Biology

pEYFP-Mito (mtYFP), mito-dsRED (mtRFP), DRP1-YFP, DRP1^{S637A}-YFP were described[5]. mt-PAGFP[46] was from M. Karbowski (University of Maryland, Baltimore, MD, USA). EPACI-camps[60] was from M. Lohse (University of Würzburg, Germany). Mt-luciferase[35] was from R. Rizzuto (University of Padova, Italy).

Two siRNA against the following target sequences from mouse mTOR were synthesized: 5′-GCGGAUGGCUCCUGACUAU-3′ and 5′-CCAAGGUGCUACAGUACUA-3′. A siRNA against the following target sequence from human mTOR was synthesized: 5′-UAACAGGUUCGAGAUAAG-3′. The scrambled control was used at the same final concentration (Dharmacon). The siRNA against human OPA1 targeted the 5′-GGACCUUAGUGAAUAUAAA-3′ sequence (Ambion).

Cell culture

SV40-transformed wt, *Mfn1*$^{-/-}$, *Mfn2*$^{-/-}$ and *DMF*$^{-/-}$ MEFs were from D. Chan and cultured as described[61]. SV40-transformed *Opa1*$^{-/-}$ and wt MEFs were a gift from C. Alexander and cultured as described[32]. SV40-transformed wt and *Drp1*$^{-/-}$ MEFs were from K. Mihara and cultured as previously described[34]. wt and *Bax*$^{-/-}$*Bak*$^{-/-}$ MEFs were cultured as described[62]. Transfection of MEFs with DNA was performed using Transfectin (Biorad), with siRNA using Oligofectamine (Invitrogen) according to manufacturer's instructions. When indicated, cells were transfected with siRNA 24 hrs after seeding on glass coverslips and with mtYFP 48hrs after plating. HeLa, HepG2 and C2C12 cells were kind gifts from C. Montecucco, A. Alberti and M. Sandri (University of Padova, Italy) and were cultured in Dulbecco's Modified Eagle Medium (DMEM, Invitrogen) supplemented with 10% fetal bovine serum (FBS, Invitrogen), 2 mM L-glutamine, non-essential amino acids (0.89 g/l L-alanine, 1.32 g/l L-asparagine, 1.33 g/l L-aspartic acid, 1.47 g/l L-glutamic acid, 0.75 g/l glycine, 1.15 g/l L-proline, 1.05 g/l L-serine, Invitrogen), 75 U/ml penicillin, 50 μg/ml streptomycin (Invitrogen) at 37°C in a 5% CO_2 atmosphere. Transfection with siRNAs and DNA was performed with Lipofectamine 2000 (Invitrogen) according to the manufacturer's protocol.

Primary hepatocytes were isolated as described[63] and cultured in DMEM (Invitrogen) supplemented with 10% FBS (Invitrogen), 1nM insulin (Sigma), 2 mM L-glutamine, non-essential amino acids (Invitrogen), , 75 U/ml penicillin, 50 μg/ml streptomycin (Invitrogen) and Fungizone (Invitrogen) at 37°C in a 5% CO_2 atmosphere.

To trigger starvation cells were washed four times and then incubated in Hanks balanced salt solution (HBSS) supplemented with 10 mM Hepes pH 7.4, at 37°C for the indicated time.

Fasting

Animal studies were performed in compliance to local animal welfare regulations. CD1 mice were fasted for 12 hrs with free access to water.

Imaging

For confocal imaging of live cells, 1.8×10^5 cells seeded onto 24-mm round glass coverslips transfected and treated as indicated were placed on the stage of a Nikon Eclipse TE300 inverted microscope equipped with a PerkinElmer Ultraview LCI confocal system, a piezoelectric z-axis motorized stage (Pifoc, Physik Instrumente, Germany), and a Orca ER 12-bit CCD camera (Hamamatsu Photonics, Japan). Cells expressing mtYFP or mtRFP were excited using the 488 nm or the 543 nm line of the HeNe laser (PerkinElmer) using a 60× 1.4 NA Plan Apo objective (Nikon).

For quantification of mitochondrial fusion rate, 2×10^5 cells seeded onto 24-mm round glass coverslips were co-transfected with mtRFP and mito-pAGFP. After 24 hrs, cells were treated as indicated and placed on the stage of a laser scanning microscope (TCS SP5, Leica). Using the LasAF software (Leica), regions of interest (ROI) to be photoactivated were manually defined. To activate the pAGFP fluorescence, 1 z-plane was activated using 100% of the power of the 413 nm laser line with a 63X, 1.4NA objective. Frames were then

acquired each min using the 488 nm and the 563 laser lines for 30 min. Standard deviation of the green fluorescence in the whole-cell was measured and normalized for the intensity of the mtRFP fluorescence using the Multi Measure plug-in of ImageJ (NIH, Bethesda).

For FRET imaging, 2×10^5 MEFs seeded onto 24-mm round glass coverslips were transfected with EPACI-camps and after 24 hrs placed on a thermostated chamber at 37°C and maintained in complete medium on the stage of an Olympus inverted microscope equipped with a CellR imaging system and a beam-splitter optical device (Multispec Microimager; Optical Insights). Sequential images of the 545 nm fluorescence emission upon excitation at 430 and 480 nm were acquired every 1 s with a 40x, 1.4 NA objective (Olympus) using the CellR software and then processed using the multi measure plug-in of Image J (National Institutes of Health, Bethesda) following background subtraction and expressed as FRET 430/480 ratio. .

Real-time imaging of mitochondrial membrane potential was performed on 1×10^5 MEFs seeded onto 24-mm round glass coverslips and loaded with TMRM, using the Olympus CellR imaging system. Imaging and analysis of TMRM fluorescence over mitochondrial regions of interest was performed as described[62].

Immunofluorescence

Primary hepatocytes were seeded onto 13-mm round glass coverslips coated with laminin. After 48 hrs cells were treated as indicated and fixed for 30 min at room temperature with 3.7% (w/V) formaldehyde, permeabilized for 20 min with ice-cold Nonidet P40 (GIBCO) and incubated with a rabbit anti-TOM20 (1:200, Santa Cruz Biotechnology). Staining was revealed with a goat anti-rabbit IgG conjugated to fluorescein-isothiocyanate (FITC) using Nikon Eclipse TE300 inverted confocal microscope and a 60x, 1.4 NA Plan Apo objective (Nikon). Stacks of 50 images separated by 0.2 μm along the z-axis were acquired. 3D reconstruction and volume rendering of the stacks were performed with the appropriate plug-in of ImageJ (National Institutes of Health, Bethesda).

Electron microscopy

MEFs of the indicated genotypes and treated as indicated were fixed with 1,25% (V/V) glutaraldehyde in 0.1 M Na-cacodylate pH 7.4 for 1 hr at room temperature. Muscle and liver specimens from mice treated as indicated were fixed in 2% formaldehyde, 2,5% (vol/vol) glutaraldehyde in 0.1 M Na-cacodylate pH 7.4 for 2 hr at room temperature and then overnight at 4°C. Electron microscopy was performed as described[10].

Morphometric and colocalization Analysis

Morphometric analysis of mitochondrial shape was performed as described[2]. For morphometric analysis of cristae biogenesis, mitochondria were randomly selected from coded samples and the number of cristae was counted and normalized for the surface of the organelle calculated by fitting a region of interest on the selected organelle using the Multi Measure plug-in of Image J (National Institutes of Health, Bethesda). Colocalization between autophagosomes and mitochondria was quantified using Manders' coefficient[30].

Isolation of mitochondria

Cells plated in 500 cm^2 plates were treated after 48 hrs as indicated and mitochondria were isolated as described[64]. Protein concentration was determined by Bradford.

Cell lysis

Cells (10^6) were harvested and disrupted in Triton X-100 lysis buffer (1% Triton X-100, 150 mM NaCl, 50 mM Tris, pH 7.4) in the presence of complete protease-inhibitor cocktail (Sigma) and phosphatase inhibitor cocktail 1 (Sigma). Protein concentration was determined by BCA assay (Pierce, Rockford, IL).

Immunoprecipitation

For immunoprecipitation, 150 μg of total cellular extract was dissolved in Triton X-100 lysis buffer and pre-cleared by centrifugation at 14000g. Fifty μl of dynabeads (Invitrogen) conjugated with protein-G were incubated with anti-DRP1 (1:50, BD Transduction) for 2 hrs at room temperature. Following 3 washes, cleared extracts were added and incubated o/n at 4°C. Beads were washed 3 times and boiled in NuPage loading buffer (Invitrogen).

Immunoblotting

The indicated amounts of proteins were separated by 4-12% Bis-Tris, 12% Bis-Tris or 7% Tris-acetate gels (NuPAGE, Invitrogen) and transferred onto polyvinylidene difluoride (PVDF, BioRad) membranes. The following antibodies were used: α-OPA1 (1:1000, BD Transduction), α-MFN1 (1:1000, Abcam), α-MFN2 (1:1000, Abcam), α-DRP1 (1:1000, BD Transduction), α-Fis1 (1:1000, Alexis), α-actin (1:30000, Chemicon), α-TOM20 (1:5000, Santa Cruz Biotechnology), α-phospho-Ser637-DRP1[5] (1:1000), α-phospho-CREB-Ser133 (1:1000, Cell Signalling), α-CREB (1:1000, Cell Signalling), α-β-tubulin (1:200, Santa Cruz Biotechnology), α-cyclophilin-D, α-MnSOD (1:5000, Stressgen), α-complex-II, subunit 70kDa (1:1000, MitoSciences), α-PMP70 (1:1000, Sigma), α-ATPase, α subunit (1:1000, MitoSciences), α-mTOR (1:1000, Cell Signalling), α-LC3 (1:200, Anaspec), α-p62 (1:5000, Progen).

Blue Native-PAGE

Cells (500 μg) were resuspended in 50 μL of native loading buffer (Invitrogen) containing 4% digitonin (Sigma) and protease-inhibitor cocktail (Sigma) After 30 min at 4°C the lysate was spun at 22000*g* for 30 min at 4°C. Four μL of native additive G250 5% (Invitrogen) was added to the supernatant and 30 μg of protein were loaded onto a 3-12% native gel (Invitrogen). Transfer of native gels was performed as described above.

In-gel ATPase activity assay

ATPase activity was measured according to[65] and ATPase activity was followed for up to 4hrs at room temperature. Gels were washed in water to stop the reaction.

ATP measurement

Total ATP levels were measured by chemiluminescence using the ATP detection assay system ATPlite (PerkinElmer), according to manufacturer's protocol. ATP levels were normalized by total protein concentration

To measure mitochondrial ATP levels during starvation, cells grown on 13 mm round glass coverslips at 50% confluence were transfected with mitochondrially targeted luciferase and after 24 hours luminescence was measured as described[35]. Basal luminescence was recorded in the absence of luciferin and then cells were perfused with 20 μM luciferin to record mitochondrial luminescence, which was then calibrated to the maximal luminescence emitted by the mt-luciferase by perfusing each sample with 10mM ATP in the presence of 100 μM digitonin.

Flow cytometry

For analysis of cell death, 4×10^4 MEFs of the indicated genotype grown in 12-well plates were treated as indicated 24 hrs after seeding. When indicated, cells were harvested and stained with propidium iodide (PI) and annexin-V-FLUOS (BenderMedSystems) according to the manufacturer's protocol. Cell viability was measured by flow cytometry (FACSCalibur, BD Biosciences) as the percentage of annexin-V and PI negative events.

For evaluation of membrane potential, 4×10^4 MEFs of the indicated genotype were grown in 12-well plates and indicated treatments (starvation) were started 36 hrs after seeding. At the indicated times, cells were harvested, washed with PBS, resuspended in HBSS supplemented with 10 mM HEPES pH 7.4 and loaded with 20 nM TMRM (Molecular Probes) in the presence of 2 mg/ml cyclosporine H, a P-glycoprotein inhibitor for 30 min at 37°C. Cells were then analyzed by flow cytometry (FACSCalibur, BD Biosciences).

Statistical tests

In each graph, unless noted, data represent mean ± SEM of the indicated number (n) of independent experiments. If indicated, statistical signficance has been calculated by a two tailed Student's *t*-test between the indicated samples. P values are indicated in the legend.

References

1. Hahn J, Voth M. Dynamics of mitochondria in living cells: shape changes, dislocations, fusion, and fission of mitochondria. Microsc. Res. Tech. 1994; 27:198–219. [PubMed: 8204911]
2. Cipolat S, de Brito OM, Dal Zilio B, Scorrano L. OPA1 requires mitofusin 1 to promote mitochondrial fusion. Proc. Natl. Acad. Sci. U. S. A. 2004; 101:15927–15932. [PubMed: 15509649]
3. Santel A, Fuller MT. Control of mitochondrial morphology by a human mitofusin. J. Cell Sci. 2001; 114:867–874. [PubMed: 11181170]
4. Smirnova E, Griparic L, Shurland DL, van der Bliek AM. Dynamin-related protein Drp1 is required for mitochondrial division in mammalian cells. Mol. Biol. Cell. 2001; 12:2245–2256. [PubMed: 11514614]
5. Cereghetti GM, et al. Dephosphorylation by calcineurin regulates translocation of Drp1 to mitochondria. Proc. Natl. Acad. Sci. U. S. A. 2008; 105:15803–15808. [PubMed: 18838687]
6. Cribbs JT, Strack S. Reversible phosphorylation of Drp1 by cyclic AMP-dependent protein kinase and calcineurin regulates mitochondrial fission and cell death. EMBO Rep. 2007; 8:939–944. [PubMed: 17721437]
7. Chang CR, Blackstone C. Cyclic AMP-dependent protein kinase phosphorylation of Drp1 regulates its GTPase activity and mitochondrial morphology. J. Biol Chem. 2007; 282:21583–21587. [PubMed: 17553808]
8. Harder Z, Zunino R, McBride H. Sumo1 conjugates mitochondrial substrates and participates in mitochondrial fission. Curr. Biol. 2004; 14:340–345. [PubMed: 14972687]
9. Braschi E, Zunino R, McBride HM. MAPL is a new mitochondrial SUMO E3 ligase that regulates mitochondrial fission. EMBO. Rep. 2009; 10:748–754. [PubMed: 19407830]
10. Scorrano L, et al. A Distinct Pathway Remodels Mitochondrial Cristae and Mobilizes Cytochrome c during Apoptosis. Dev. Cell. 2002; 2:55–67. [PubMed: 11782314]
11. Martinou I, et al. The release of cytochrome c from mitochondria during apoptosis of NGF-deprived sympathetic neurons is a reversible event. J. Cell Biol. 1999; 144:883–889. [PubMed: 10085288]
12. Frank S, et al. The role of dynamin-related protein 1, a mediator of mitochondrial fission, in apoptosis. Dev. Cell. 2001; 1:515–525. [PubMed: 11703942]
13. Szabadkai G, et al. Drp-1-dependent division of the mitochondrial network blocks intraorganellar Ca^{2+} waves and protects against Ca^{2+}-mediated apoptosis. Mol Cell. 2004; 16:59–68. [PubMed: 15469822]

14. Li Z, Okamoto K, Hayashi Y, Sheng M. The importance of dendritic mitochondria in the morphogenesis and plasticity of spines and synapses. Cell. 2004; 119:873–887. [PubMed: 15607982]
15. Campello S, et al. Orchestration of lymphocyte chemotaxis by mitochondrial dynamics. J. Exp. Med. 2006; 203:2879–2886. [PubMed: 17145957]
16. Mitra K, Wunder C, Roysam B, Lin G, Lippincott-Schwartz J. A hyperfused mitochondrial state achieved at G1-S regulates cyclin E buildup and entry into S phase. Proc. Natl. Acad. Sci. U. S. A. 2009; 106:11960–11965. [PubMed: 19617534]
17. Scheckhuber CQ, et al. Reducing mitochondrial fission results in increased life span and fitness of two fungal ageing models. Nat. Cell Biol. 2007; 9:99–105. [PubMed: 17173038]
18. Twig G, et al. Fission and selective fusion govern mitochondrial segregation and elimination by autophagy. EMBO J. 2008; 27:433–446. [PubMed: 18200046]
19. Gomes LC, Scorrano L. High levels of Fis1, a pro-fission mitochondrial protein, trigger autophagy. Biochim. Biophys. Acta. 2008; 1777:860–866. [PubMed: 18515060]
20. Klionsky DJ, Emr SD. Autophagy as a regulated pathway of cellular degradation. Science. 2000; 290:1717–1721. [PubMed: 11099404]
21. Cecconi F, Levine B. The role of autophagy in mammalian development: cell makeover rather than cell death. Dev. Cell. 2008; 15:344–357. [PubMed: 18804433]
22. Ravikumar B, Duden R, Rubinsztein DC. Aggregate-prone proteins with polyglutamine and polyalanine expansions are degraded by autophagy. Hum. Mol. Genet. 2002; 11:1107–1117. [PubMed: 11978769]
23. Zheng YT, et al. The adaptor protein p62/SQSTM1 targets invading bacteria to the autophagy pathway. J Immunol. 2009; 183:5909–5916. [PubMed: 19812211]
24. Tuttle DL, Lewin AS, Dunn WA Jr. Selective autophagy of peroxisomes in methylotrophic yeasts. Eur. J Cell Biol. 1993; 60:283–290. [PubMed: 8330626]
25. Bernales S, McDonald KL, Walter P. Autophagy Counterbalances Endoplasmic Reticulum Expansion during the Unfolded Protein Response. PLoS Biol. 2006; 4:e423. [PubMed: 17132049]
26. Elmore SP, Qian T, Grissom SF, Lemasters JJ. The mitochondrial permeability transition initiates autophagy in rat hepatocytes. FASEB J. 2001; 15:2286–2287. [PubMed: 11511528]
27. Tooze SA, Yoshimori T. The origin of the autophagosomal membrane. Nat Cell Biol. 2010; 12:831–835. [PubMed: 20811355]
28. Scherz-Shouval R, et al. Reactive oxygen species are essential for autophagy and specifically regulate the activity of Atg4. EMBO J. 2007; 26:1749–1760. [PubMed: 17347651]
29. Hailey DW, et al. Mitochondria supply membranes for autophagosome biogenesis during starvation. Cell. 2010; 141:656–667. [PubMed: 20478256]
30. de Brito OM, Scorrano L. Mitofusin 2 tethers endoplasmic reticulum to mitochondria. Nature. 2008; 456:605–610. [PubMed: 19052620]
31. Karbowski M, et al. Quantitation of mitochondrial dynamics by photolabeling of individual organelles shows that mitochondrial fusion is blocked during the Bax activation phase of apoptosis. J. Cell Biol. 2004; 164:493–499. [PubMed: 14769861]
32. Song Z, Chen H, Fiket M, Alexander C, Chan DC. OPA1 processing controls mitochondrial fusion and is regulated by mRNA splicing, membrane potential, and Yme1L. J. Cell Biol. 2007; 178:749–755. [PubMed: 17709429]
33. Chen H, Chomyn A, Chan DC. Disruption of fusion results in mitochondrial heterogeneity and dysfunction. J. Biol. Chem. 2005; 280:26185–26192. [PubMed: 15899901]
34. Ishihara N, et al. Mitochondrial fission factor Drp1 is essential for embryonic development and synapse formation in mice. Nat. Cell Biol. 2009; 11:958–966. [PubMed: 19578372]
35. Jouaville LS, Pinton P, Bastianutto C, Rutter GA, Rizzuto R. Regulation of mitochondrial ATP synthesis by calcium: evidence for a long-term metabolic priming. Proc. Natl. Acad. Sci. U. S. A. 1999; 96:13807–13812. [PubMed: 10570154]
36. Rich P. Chemiosmotic coupling: The cost of living. Nature. 2003; 421:583. [PubMed: 12571574]
37. Strauss M, Hofhaus G, Schroder RR, Kuhlbrandt W. Dimer ribbons of ATP synthase shape the inner mitochondrial membrane. EMBO J. 2008; 27:1154–1160. [PubMed: 18323778]

38. Giraud MF, et al. Is there a relationship between the supramolecular organization of the mitochondrial ATP synthase and the formation of cristae? Biochim. Biophys. Acta. 2002; 1555:174–180. [PubMed: 12206911]
39. Unger RH. Glucagon physiology and pathophysiology in the light of new advances. Diabetologia. 1985; 28:574–578. [PubMed: 3902546]
40. Pan X, Heitman J. Cyclic AMP-Dependent Protein Kinase Regulates Pseudohyphal Differentiation in Saccharomyces cerevisiae. Mol. Cell. Biol. 1999; 19:4874–4887. [PubMed: 10373537]
41. Budovskaya YV, Stephan JS, Reggiori F, Klionsky DJ, Herman PK. The Ras/cAMP-dependent protein kinase signaling pathway regulates an early step of the autophagy process in Saccharomyces cerevisiae. J Biol. Chem. 2004; 279:20663–20671. [PubMed: 15016820]
42. Stephan JS, Yeh YY, Ramachandran V, Deminoff SJ, Herman PK. The Tor and PKA signaling pathways independently target the Atg1/Atg13 protein kinase complex to control autophagy. PNAS. 2009; 106:17049–17054. [PubMed: 19805182]
43. Mavrakis M, Lippincott-Schwartz J, Stratakis CA, Bossis I. Depletion of type IA regulatory subunit (RIalpha) of protein kinase A (PKA) in mammalian cells and tissues activates mTOR and causes autophagic deficiency. Hum. Mol Genet. 2006; 15:2962–2971. [PubMed: 16963469]
44. Slattery MG, Liko D, Heideman W. Protein Kinase A, TOR, and Glucose Transport Control the Response to Nutrient Repletion in Saccharomyces cerevisiae. Eukaryotic Cell. 2008; 7:358–367. [PubMed: 18156291]
45. Tondera D, et al. SLP-2 is required for stress-induced mitochondrial hyperfusion. EMBO. J. 2009; 28:1589–1600. [PubMed: 19360003]
46. Karbowski M, Youle RJ. Dynamics of mitochondrial morphology in healthy cells and during apoptosis. Cell Death. Differ. 2003; 10:870–880. [PubMed: 12867994]
47. Cereghetti GM, Costa V, Scorrano L. Inhibition of Drp1-dependent mitochondrial fragmentation and apoptosis by a polypeptide antagonist of calcineurin. Cell Death Differ. 2010; 17:1785–1794. [PubMed: 20489733]
48. Wasiak S, Zunino R, McBride HM. Bax/Bak promote sumoylation of DRP1 and its stable association with mitochondria during apoptotic cell death. J. Cell Biol. 2007; 177:439–450. [PubMed: 17470634]
49. Nakamura N, Kimura Y, Tokuda M, Honda S, Hirose S. MARCH-V is a novel mitofusin 2-and Drp1-binding protein able to change mitochondrial morphology. EMBO. Rep. 2006; 7:1019–1022. [PubMed: 16936636]
50. Karbowski M, Neutzner A, Youle RJ. The mitochondrial E3 ubiquitin ligase MARCH5 is required for Drp1 dependent mitochondrial division. J. Cell Biol. 2007; 178:71–84. [PubMed: 17606867]
51. Tanaka A, et al. Proteasome and p97 mediate mitophagy and degradation of mitofusins induced by Parkin. J Cell Biol. 2010; 191:1367–1380. [PubMed: 21173115]
52. Ziviani E, Tao RN, Whitworth AJ. Drosophila parkin requires PINK1 for mitochondrial translocation and ubiquitinates mitofusin. Proc. Natl. Acad. Sci. U. S. A. 2010; 107:5018–5023. [PubMed: 20194754]
53. Narendra D, Tanaka A, Suen DF, Youle RJ. Parkin is recruited selectively to impaired mitochondria and promotes their autophagy. J. Cell. Biol. 2008; 183:795–803. [PubMed: 19029340]
54. Costa V, et al. Mitochondrial fission and cristae disruption increase the response of cell models of Huntington's disease to apoptotic stimuli. EMBO Mol Med. 2010; 2:490–503. [PubMed: 21069748]
55. Brown GC. Control of respiration and ATP synthesis in mammalian mitochondria and cells. Biochem. J. 1992; 284(Pt 1):1–13. [PubMed: 1599389]
56. Frezza C, et al. OPA1 Controls Apoptotic Cristae Remodeling Independently from Mitochondrial Fusion. Cell. 2006; 126:177–189. [PubMed: 16839885]
57. Meeusen S, et al. Mitochondrial inner-membrane fusion and crista maintenance requires the dynamin-related GTPase Mgm1. Cell. 2006; 127:383–395. [PubMed: 17055438]
58. Mopert K, et al. Loss of Drp1 function alters OPA1 processing and changes mitochondrial membrane organization. Exp. Cell. Res. 2009; 315:2165–2180. [PubMed: 19409380]

59. Kuma A, et al. The role of autophagy during the early neonatal starvation period. Nature. 2004; 432:1032–1036. [PubMed: 15525940]

60. Nikolaev VO, B++nemann M, Hein L, Hannawacker A, Lohse MJ. Novel Single Chain cAMP Sensors for Receptor-induced Signal Propagation. J. Biol. Chem. 2004; 279:37215–37218. [PubMed: 15231839]

61. de Brito OM, Scorrano L. Mitofusin 2 tethers endoplasmic reticulum to mitochondria. Nature. 2008; 456:605–610. [PubMed: 19052620]

62. Scorrano L, et al. BAX and BAK regulation of endoplasmic reticulum Ca^{2+}: a control point for apoptosis. Science. 2003; 300:135–139. [PubMed: 12624178]

63. Danial NN, et al. BAD and glucokinase reside in a mitochondrial complex that integrates glycolysis and apoptosis. Nature. 2003; 424:952–956. [PubMed: 12931191]

64. Frezza C, Cipolat S, Scorrano L. Organelle isolation: functional mitochondria from mouse liver, muscle and cultured fibroblasts. Nat. Protoc. 2007; 2:287–295. [PubMed: 17406588]

65. Alirol E, et al. The mitochondrial fission protein hFis1 requires the endoplasmic reticulum gateway to induce apoptosis. Mol. Biol. Cell. 2006; 17:4593–4605. [PubMed: 16914522]

Europe PMC Funders Author Manuscripts

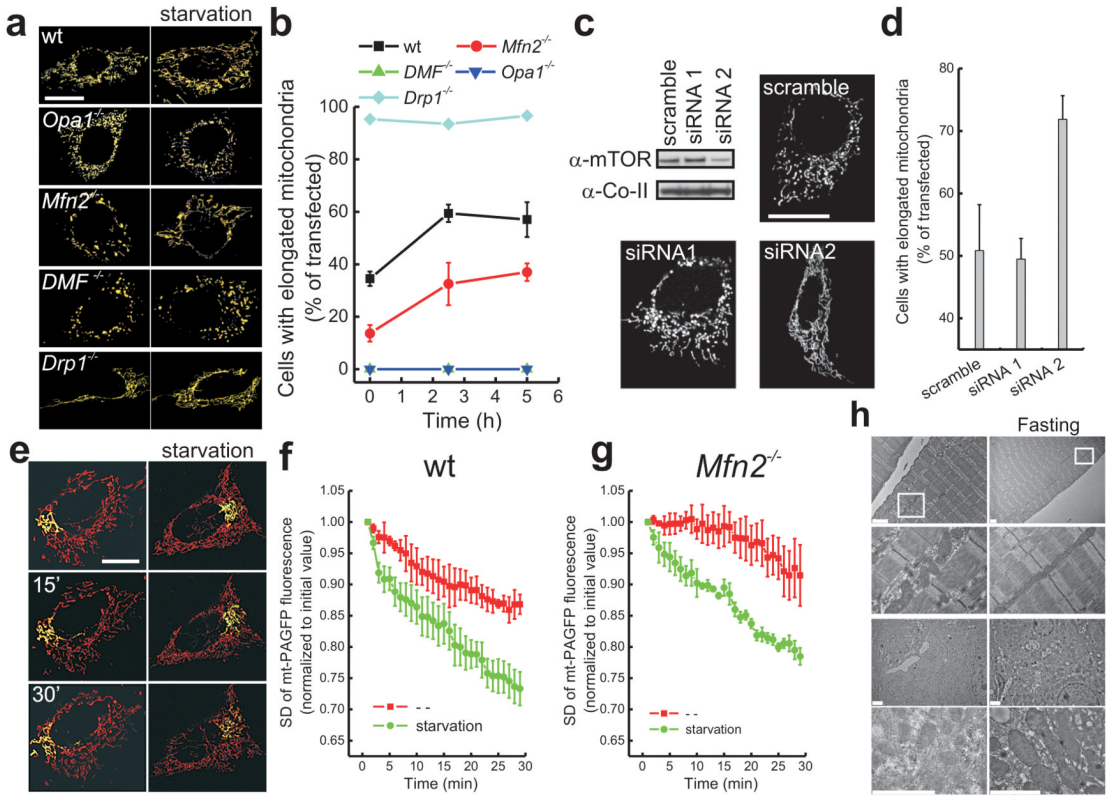

Figure 1. Mitochondrial elongation in response to autophagy

(a) Representative confocal images of mitochondrial morphology in MEFs of the indicated genotype 24 hrs following transfection with mtYFP. Where indicated, cells were starved for 2.5 hrs. Bar, 20 μm

(b) Morphometric analysis of mitochondrial shape. Experiments were carried exactly as in (a). Data represent mean ± SEM of 3 independent experiments (n=100 cells per condition in each experiment).

(c) Forty-eight hrs after transfection with the indicated siRNA MEFs were lysed and 25 μg of proteins were separated by SDS-PAGE and immunoblotted with the indicated antibodies. Representative images show mitochondrial morphology of MEFs transfected with the indicated siRNA and after 24 hrs with mtYFP. After further 24 hrs confocal images were acquired. Bar, 20 μm.

(d) Morphometric analysis of mitochondrial shape. Experiments were carried exactly as in (c). Data represent mean ± SEM of 5 independent experiments (n=100 cells per condition in each experiment).

(e) Representative images of mitochondrial fusion. MEFs were co-transfected with mt-PAGFP and mtRFP and after 24 hrs, mt-PAGFP was photoactivated in a region of interest (box) and cells were imaged by real time confocal microscopy. Where indicated, MEFs were starved for 2.5 hrs. Bar, 20 μm. See also Supplementary Movies 1-2

(f-g) Quantification of mitochondrial fusion in MEFs of the indicated genotype. Experiments were carried exactly as in (e). Data represent mean ± SEM of 4 independent experiments.

(h) Representative electron micrographs of muscle (longitudinal sections) and liver from CD1 mice. Where indicated, mice were fasted for 12 hrs. Magnifications of boxed regions are presented below. Bar, 2 μm.

Europe PMC Funders Author Manuscripts

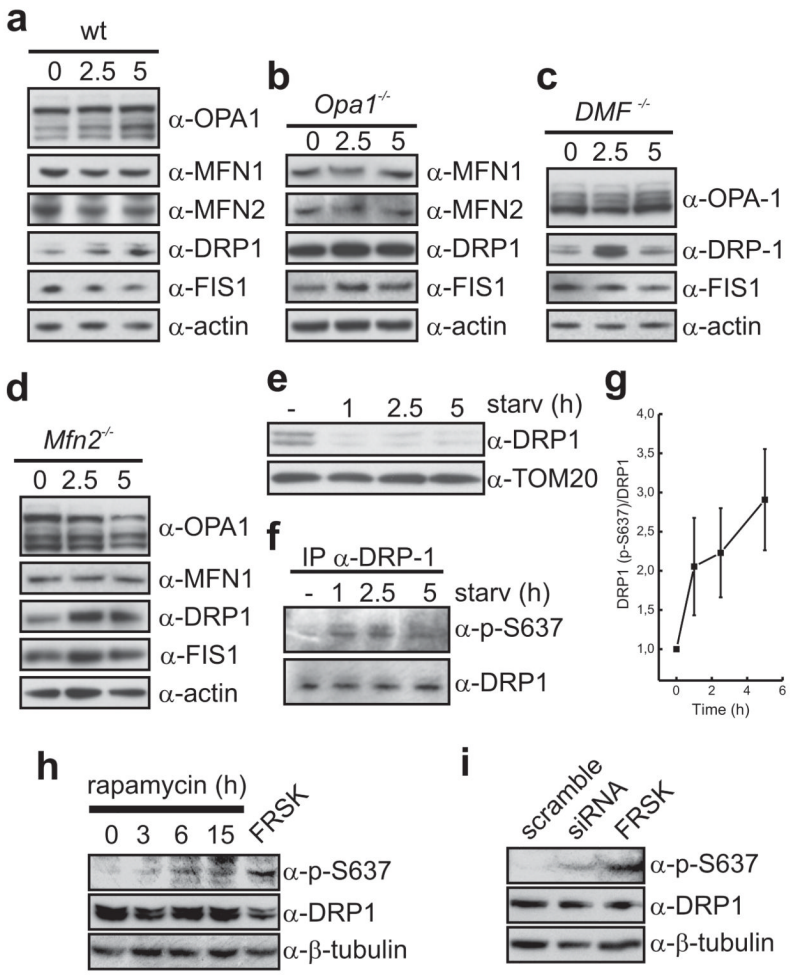

Figure 2. Increased phosphorylation of Ser637 of DRP1 during autophagy

(a-d) Levels of mitochondria-shaping proteins during starvation. Twenty μg of proteins from MEFs of the indicated genotype were separated by SDS-PAGE and immunoblotted with the indicated antibodies. Where indicated, cells were starved for the indicated times.

(e) Association of DRP1 with mitochondria upon starvation. Mitochondria were isolated from MEFs starved for the indicated times and 25 μg of proteins were separated by SDS-PAGE and immunoblotted with the indicated antibodies.

(f) Levels of Ser-637 phosphorylation of DRP1 during starvation. Equal amounts of cell lysates from wt MEFs starved for the indicated times were immunoprecipitated with the indicated antibody and the immunoprecipitated proteins were separated by SDS-PAGE and immunoblotted with the indicated antibodies.

(g) Quantitative analysis of Ser-637 phosphorylation of DRP1 during starvation. Experiments were as in (l). Data are normalized to total levels of DRP1 and represent the mean ±SEM of 3 independent experiments.

(h) MEFs were treated for the indicated times with 100 nM rapamycin or with 25 μM forskolin for 0.5 hrs, lysed and equal amounts (50 μg) of proteins were separated by SDS-PAGE and immunoblotted using the indicated antibodies.

(i) HeLa cells were transfected for 2 days with the indicated siRNA or treated with 25 μM forskolin for 0.5 hrs and lysed. Equal amounts (50 μg) of proteins were separated by SDS-PAGE and immunoblotted using the indicated antibodies. Uncropped images of all blots in this figure are shown in Supplementary Information, Fig. S8.

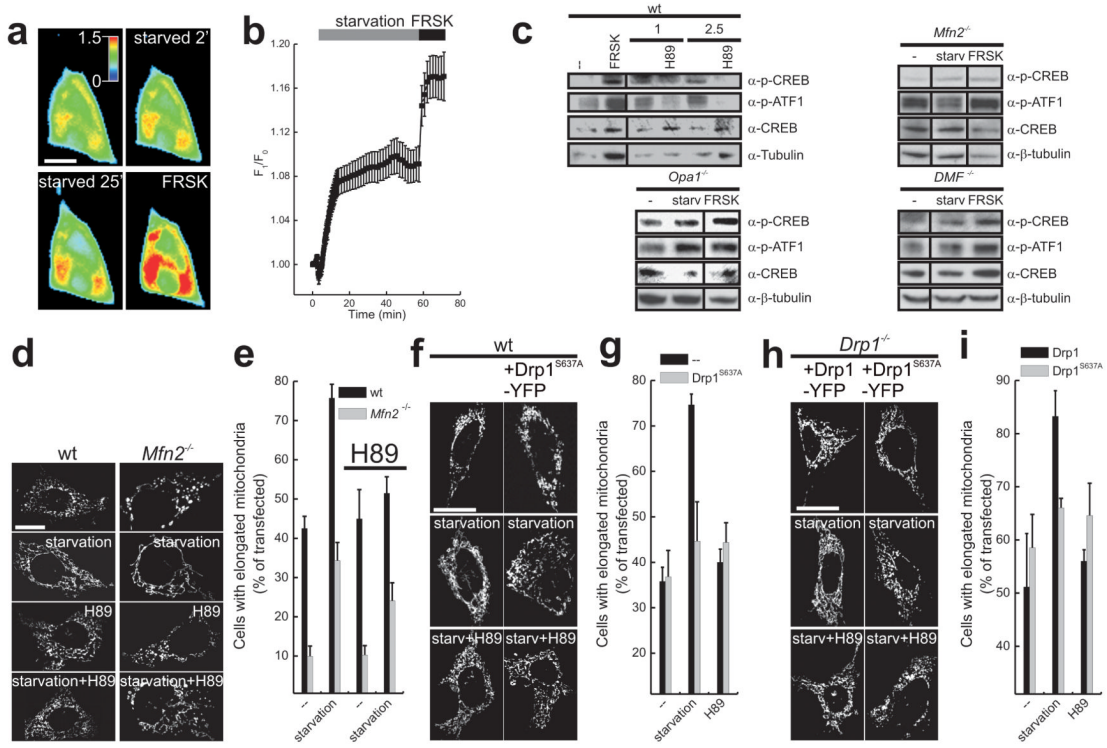

Figure 3. Mitochondrial elongation during starvation is mediated by the cAMP-PKA axis

(a) Pseudocolor-coded images of EpacI-camps FRET from real time imaging of wt MEFs transfected with EpacI-camps. Where indicated, cells where perfused with the starvation solution for the indicated times or with 25 μM forskolin. Bar, 20 μm. See also Supplementary Movie 3

(b) Quantitative analysis of CFP/YFP FRET ratio. Experiments were as in (a). Where indicated, cells were perfused with the starvation solution or with 25 μM forskolin. Data represent mean ± SEM of 13 independent experiments.

(c) Fifty μg of lysates of MEFs of the indicated genotypes were analyzed by SDS-PAGE/ immunoblotting using the indicated antibodies. Where indicated, MEFs were starved, or treated with 25 μM forskolin (FRSK). Where indicated, 20 μM H89 was added during starvation. Uncropped images of all blots in this figure are shown in Supplementary Information, Fig. S8.

(d) Representative images of the effect of H89 on mitochondrial morphology upon starvation. wt and *Mfn2*$^{-/-}$ MEFs were transfected with mtYFP, and after 24 hrs confocal images were acquired. Where indicated, cells were starved for 2.5 hrs and 20 μM H89 was added. Bar, 20 μm.

(e) Morphometric analysis. Experiments were carried exactly as in (d). Data represent mean ± SEM of 5 independent experiments (n=100 cells per condition).

(f) Starvation-induced mitochondrial elongation depends on Ser 637 of DRP1. Representative confocal images of mitochondrial morphology of wt MEFs co-transfected with mtRFP and the indicated plasmids. Twenty-four hrs after transfection, where indicated cells were starved for 2.5 hrs and imaged. Where indicated, 20 μM H89 was present during starvation. Bar, 20 μm.

(g) Morphometric analysis of mitochondrial shape. Experiments were as in (f). Data represent mean ± SEM of 5 independent experiments (n= 50 cells per condition).

(h) Representative confocal images of mitochondrial morphology of *Drp1*$^{-/-}$ MEFs co-transfected with mtRFP and the indicated plasmids. Twenty-four hrs after transfection,

Europe PMC Funders Author Manuscripts

where indicated cells were starved for 2.5 hrs and imaged. Where indicated, 20 μM H89 was present during starvation. Bar, 20 μm.

(i) Morphometric analysis of mitochondrial shape. Experiments were as in (h). Data represent mean ± SEM of 5 independent experiments (n= 50 cells per condition).

Europe PMC Funders Author Manuscripts

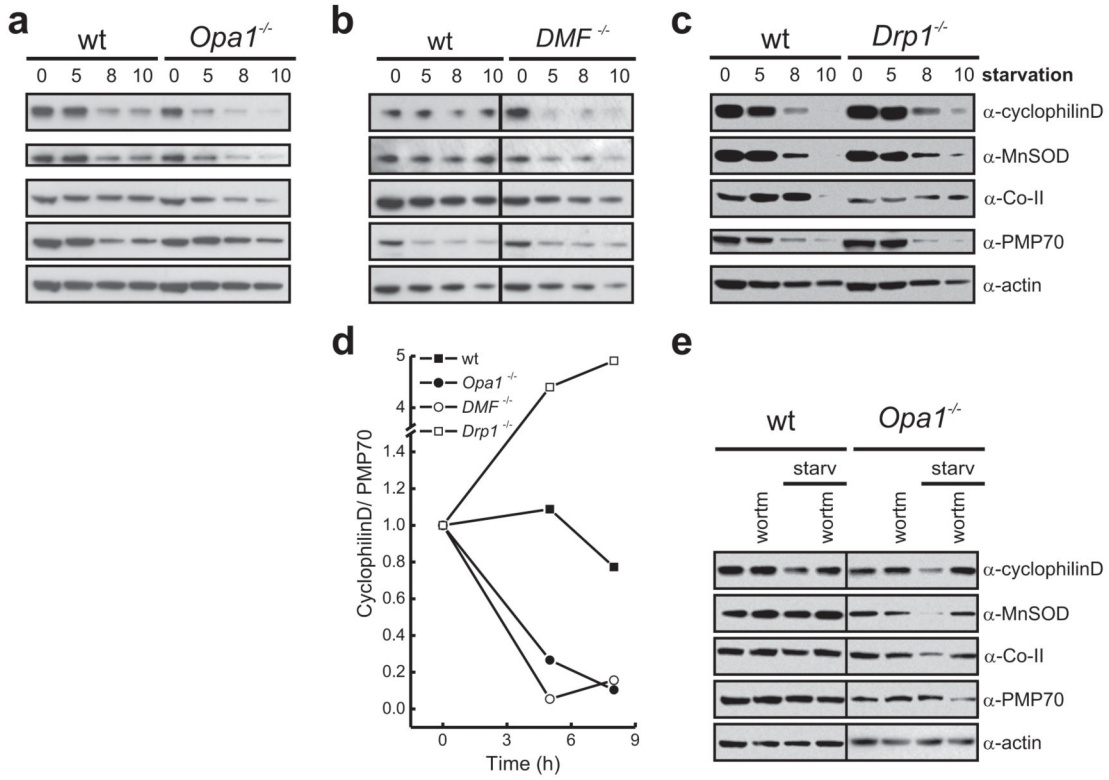

Figure 4. Elongated mitochondria are spared from degradation during starvation

(a-c) MEFs of the indicated genotype were treated as indicated, counted and 2.7×10^5 cells were lysed. Lysates were separated by SDS-PAGE and immunoblotted using the indicated antibodies.

(d) Ratio between the densitometric levels of cyclophilin D and those of PMP70 in MEFs of the indicated genotype. One representative experiment of 5 independent repetitions carried as in (a-c) is shown.

(e) MEFs of the indicated genotype starved for 5h were treated where indicated with 0.5 μM wortmannin (wortm). Lysates from 2.7×10^5 cells were separated by SDS-PAGE and immunoblotted with the indicated antibodies. Uncropped images of all blots in this figure are shown in Supplementary Information, Fig. S8.

Europe PMC Funders Author Manuscripts

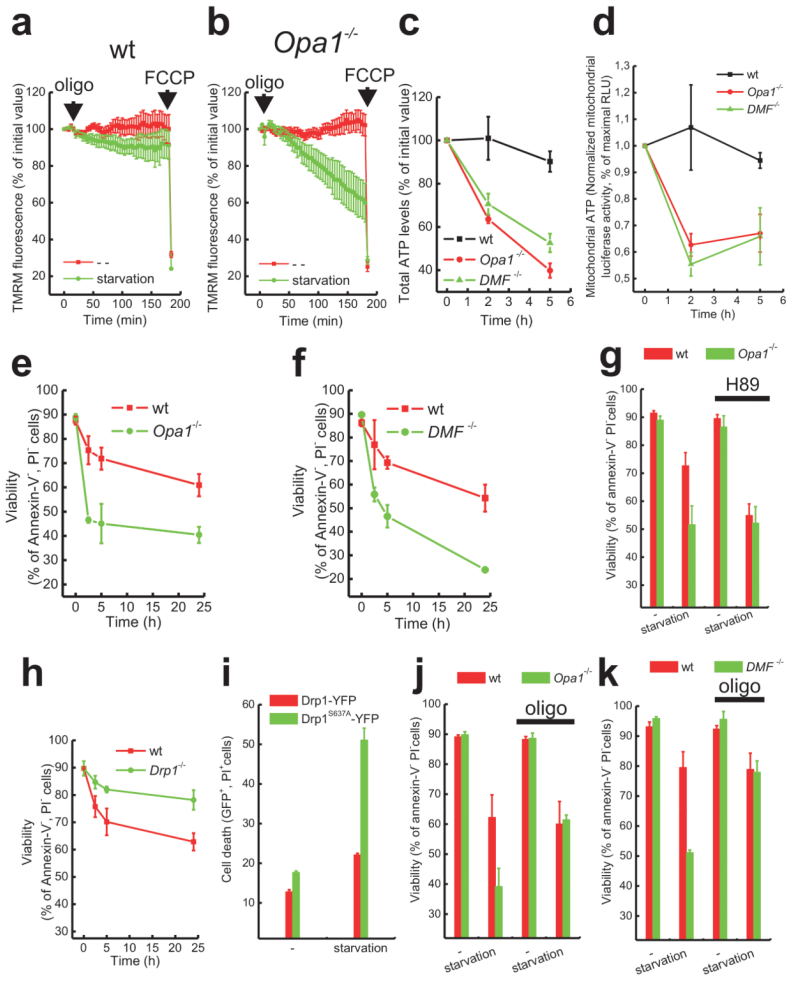

Figure 5. Mitochondrial elongation sustains cellular ATP production and viability during autophagy

(a,b) Quantitative analysis of TMRM fluorescence changes over mitochondrial regions in MEFs of the indicated genotype. Where indicated, cells were starved for 5 hrs prior to TMRM loading. Where indicated (arrows), 2.5 μg/ml oligomycin and 2 μM FCCP were added. Data represent mean ± SEM of 7 independent experiments.

(c) Total cellular ATP levels were measured in cells of the indicated genotype starved for the indicated times. Data represent mean ± SEM of 5 independent experiments.

(d) Mitochondrial ATP measured in situ by mitochondrially targeted luciferase in cells of the indicated genotype starved for the indicated times. Data represent mean ± SEM of 5 independent experiments and are normalized to the initial value.

(e,f) Cells of the indicated genotype were starved for the indicated times and viability was determined by flow cytometry. Data represent mean ± SEM of 5 independent experiments.

(g) MEFs of the indicated genotype were starved for 2.5 hrs. Where indicated, cells were treated with 20 μM H89. Viability was determined by flow cytometry. Data represent mean ± SEM of 5 independent experiments.

(h) Cells of the indicated genotype were starved for the indicated times and viability was determined by flow cytometry. Data represent mean ± SEM of 5 independent experiments.

(i) *Drp1*$^{-/-}$ MEFs were transfected with the indicated plasmids and after 24 hrs starved for 5 hrs where indicated. Viability was determined by flow cytometry. Data represent mean ± SEM of 4 independent experiments.

Europe PMC Funders Author Manuscripts

(j,k) MEFs of the indicated genotype were starved for 5 hrs in the presence of 2.5μg/mL oligomycin where indicated and viability was determined cytofluorimetrically. Data represent mean ± SEM of 5 independent experiments.

Europe PMC Funders Author Manuscripts

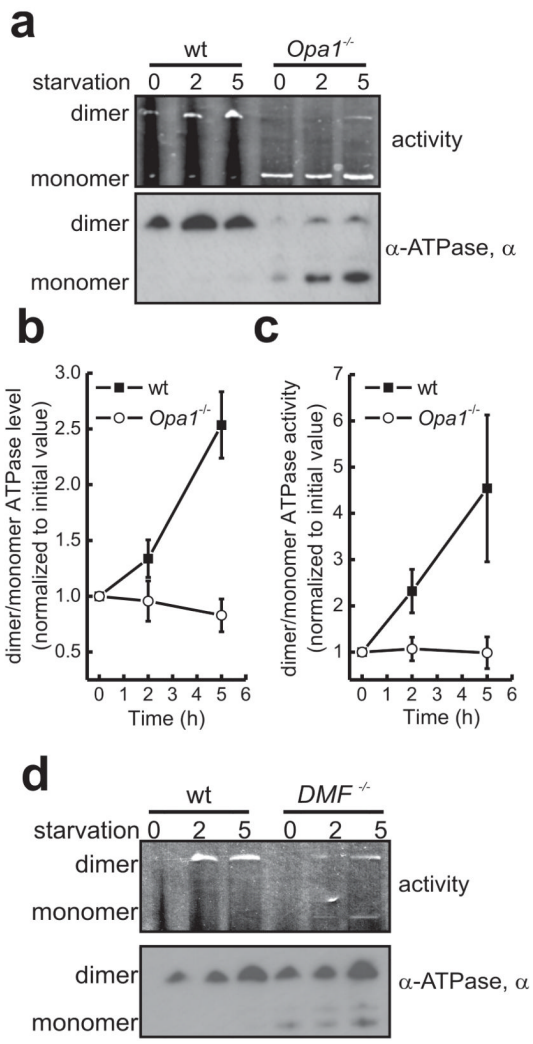

Figure 6. Mitochondrial elongation during starvation is associated with dimerization and activation of ATPase

(**a**) Blue native electrophoresis analysis of ATPase dimerization and activity. Cells of the indicated genotype were treated as indicated and 500 μg of total cell extracts were solubilized with 4% digitonin and separated by BN-PAGE. ATPase activity was measured in gel (top) and ATPase levels were measured by immunoblotting for the indicated antibody (middle).

(**b-c**) Quantitative analysis of levels (b) and activity (c) of the ratio between dimer and monomer of ATPase. Data represent mean ± SEM of 5 independent experiments carried as in (a).

(d) Experiments were carried out as in (a), except that cells of the indicated genotype were used.

Europe PMC Funders Author Manuscripts

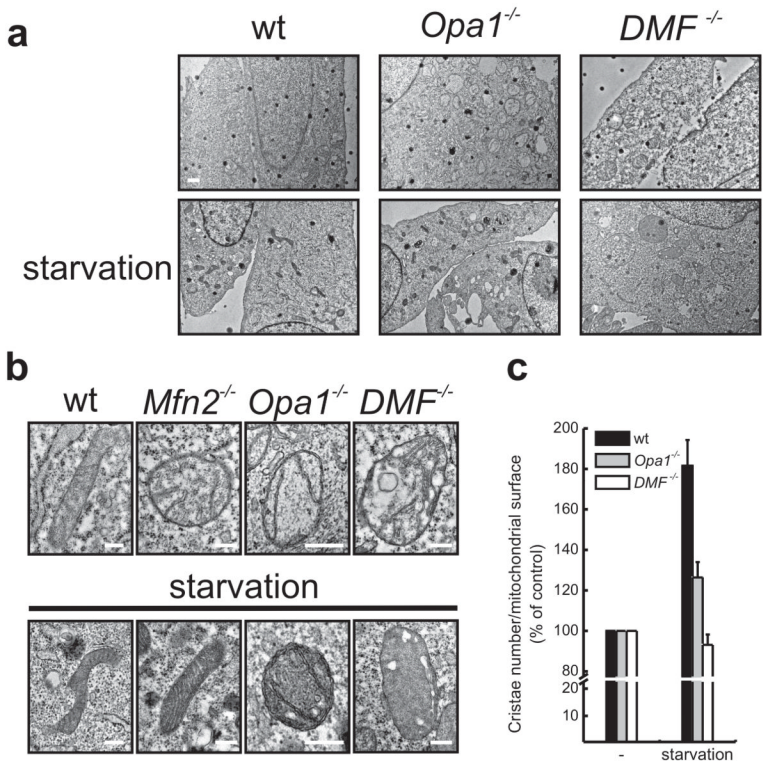

Figure 7. Density of cristae increases in mitochondria elongated during starvation

(a) Representative electron micrographs of cells of the indicated genotype starved where indicated for 5h, fixed and processed for electron microscopy. Bar 2 μm.

(b) Representative electron micrographs of randomly selected mitochondria from cells of the indicated genotype. Where indicated, cells were starved for 5h. Bar, 0.5 μm.

(c) Morphometric analysis of cristae density in cells of the indicated genotype. Experiments were as in (a). The number of the cristae in randomly selected 50 mitochondria of the indicated genotype was normalized for the calculated surface of the organelle. Data represent mean ± SEM of 5 independent experiments.

Europe PMC Funders Author Manuscripts

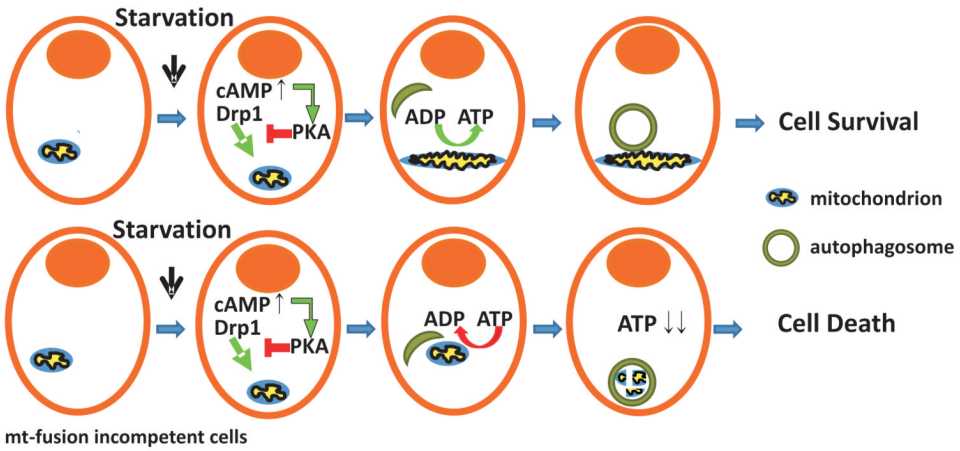

Figure 8. Mitochondrial elongation induced by PKA determines cell fate during starvation

The cartoon depicts the cascade of mitochondrial elongation triggered during starvation and its role in determining cell fate. Upper row: mitochondrial elongation protects from organelle degradation and allows maintenance of ATP levels. Lower row: when mitochondrial elongation is impaired, mitochondria are degraded and the remaining organelles consume cellular ATP, precipitating cell death.

Europe PMC Funders Author Manuscripts